Hyperfine structure of the 2s state of $^3He^+$ †

M. H. Prior and E. C. Wang
University of California, Lawrence Berkeley Laboratory, Berkeley, California 94720
(Received 2 February 1977)

Using an electrostatic ion-storage device and a microwave state-selection technique, we have measured the hyperfine structure $\Delta\nu_2$ of the $2s$ state of $^3He^+$. Our result is $\Delta\nu_2 = 1083.354\,980\,7(88)$ MHz (the equivalent uncertainty is 0.009 ppm). When combined with the $1s$-state hyperfine structure $\Delta\nu_1$ to make the quantity $D_{21} \equiv 8\Delta\nu_2 - \Delta\nu_1$, we obtain D_{21}(experiment) = 1.189 979(71) MHz. Current theory produces D_{21}(theory) = 1.189 801(1) MHz. The 178(71) Hz difference may arise from a combination of quantum-electrodynamic and nuclear structure effects which remain to be treated theoretically.

I. INTRODUCTION

One of the most precisely measured quantities in atomic physics is the hyperfine structure (hfs) in the ground-state of the hydrogen atom. This quantity, with a fractional uncertainty[1] of 1.4×10^{-12}, is a strong challenge to theory in the one-electron atom. Unfortunately, theory is blocked at the level of about 5 ppm by uncertainty in the combined nuclear size and polarizability contributions (34.6 ppm) to the hyperfine energy.[2,3] Thus there are many interesting corrections to simple theory which are of the same size or smaller than the uncertainty in these nuclear effects which cannot be tested by direct comparison with the experimental value. Alternatively, one is blocked from improving the fine-structure constant α by equating the theoretical expression for the hfs to the experimental value.

It is possible to get around the nuclear structure problem, at least in part, if one has available an additional precision hfs measurement in an excited state. For practical reasons this is restricted to $\Delta\nu_2$, the metastable $2s$-state hfs. Together with $\Delta\nu_1$, the $1s$ hfs, one forms the difference $D_{21} \equiv 8\Delta\nu_2 - \Delta\nu_1$, which is much less sensitive to nuclear structure than $\Delta\nu_1$ or $\Delta\nu_2$ separately. Thus, a good experimental test of the terms contributing to D_{21} is possible. Precise measurements of $\Delta\nu_1$ and $\Delta\nu_2$ exist for H (Refs. 1 and 4), D (Refs. 5 and 6), and $^3He^+$ (Refs. 8 and 9); in this work we report an improvement in $\Delta\nu_2$ for the latter. The precision of the $\Delta\nu_2$ measurements is far short of that for $\Delta\nu_1$ in hydrogen; they are good enough, however, to give utility to the D_{21} comparison scheme. For technical reasons, $^3He^+$ provides the more precise experimental value for D_{21}.

In $^3He^+$, $\Delta\nu_1$ has been measured to high accuracy by Schuessler, Fortson, and Dehmelt[7] using an ion-storage technique; their result is $\Delta\nu_1 = 8665.649\,867(10)$ MHz. $\Delta\nu_2$ was first measured using an ion-beam technique by Commins and Novick;[8] they obtained $\Delta\nu_2 = 1083.354\,99(20)$ MHz. Recently we reported[9] preliminary results of our current work which gave a result for $\Delta\nu_2$ in agreement with Commins and Novick but with about one seventh their uncertainty (i.e., ±30 Hz). In this report, we give a result which is further improved with an uncertainty of ± 9 Hz (0.009 ppm), and explain in more detail our experimental method.

II. EXPERIMENTAL METHOD

We have used the same method described previously[9] with some improvements to increase the signal count rate and hence raise the signal-to-noise ratio for the resonance curves. Figure 1 shows an energy level diagram of the $^3He^+$ ion in the $2s$ and $2\,^2P_{1/2}$ states. Our method consists of creating $2s$ ions inside an ion-confinement device

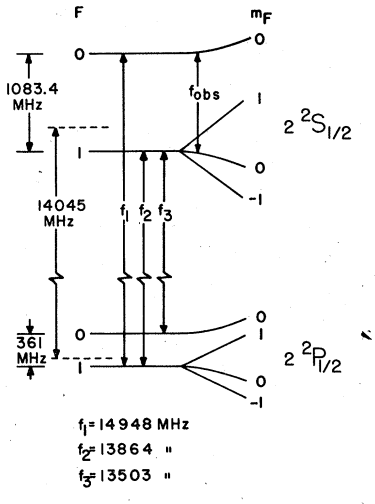

FIG. 1. Hyperfine and Zeeman levels of $^3He^+$ $2s$ and $2\,^2P_{1/2}$ states. The $2\,^2P_{1/2}$ levels have a lifetime of 10^{-10} sec and emit a 304-Å photon in decay to the ground state. The $2s$ levels have a lifetime of about 2 msec. The transition studied is marked f_{obs}

(ion trap) by electron impact on ^{3}He gas at low pressure (about 4.0×10^{-6} Torr). While the ions are confined, we preferentially remove those in either the $F=0$ or $F=1$ hyperfine states by application of a microwave power pulse tuned near the hyperfine split Lamb shift transitions f_1 or f_2, f_3 (the large width of the $2\,^2P_{1/2}$ state causes the f_2 and f_3 resonances to be unresolved). Once in the $2\,^2P_{1/2}$ state, an ion decays very rapidly (10^{-10} sec) to the ground state, emitting a 304-Å photon. Population of the depleted hyperfine level can be restored by transfer from the undepleted level via the $F=1$, $\Delta m_F=0$ hyperfine transition marked f_{obs} in Fig. 1. This is done following the microwave state selection by application of a suitably polarized oscillating magnetic field pulse near the hfs frequency. A second microwave pulse is then applied and photon detectors and associated electronics count the number of ensuing 304-Å photons. Counts collected versus frequency applied during the middle period yield a resonance curve, ideally at the unperturbed hfs frequency, $\Delta\nu_2$.

This is the same state-selection and resonance detection scheme used in the ion-beam experiment of Novick and Commins,[8] the difference being temporal separation of the functions rather than spatial separation. In analogy to atomic beam nomenclature (i.e., A, C, and B magnets), we denote the three sequential time intervals in our experiment as t_A, t_C, and t_B. The advantage of our method lies in the considerably longer values of t_C available to us compared to the C-region transit time of the 20-eV ion beam. This has allowed us to achieve linewidths for the hfs resonance of about 1.0 kHz whereas the narrowest linewidth achieved with the ion beam was about 100 kHz. The precision of a resonance line-center determination can be roughly estimated as the linewidth (full width at half maximum) divided by the signal-to-noise ratio. We have not achieved as high a signal-to-noise ratio for our resonance signals as was achieved by the ion-beam technique, thus we do not gain the full factor of 100 improvement in precision that the linewidth reduction might indicate. We have been able to locate our line centers to about 1/100 of their width, whereas in the ion-beam experiment this factor was about 1/500; our net gain in precision is thus about a factor of 20.

It was our intention to try to obtain an experimental configuration which would produce resonances at the essentially field-free hyperfine frequency in order to avoid the need for large corrections and extrapolations. For this reason we did not choose to use a Penning-type ion trap such as that used previously[10] to measure the $2s$ lifetime in $^4He^+$. The magnetic field associated with this

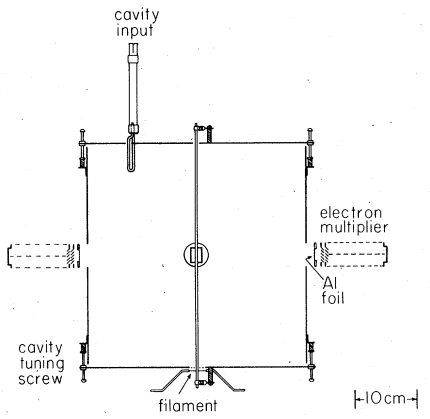

FIG. 2. Cylindrical electrostatic ion-trap/rf cavity and photon detectors. The rod on the axis is maintained at a negative potential during ion confinement. The rectangular shape shown behind the rod center is the microwave horn used to induce $2s$ to $2p_{1/2}$ transitions.

type of device would have required a large Zeeman-effect correction. The large dynamic electric fields associated with radio-frequency quadrupole ion traps[11] were considered prohibitive because of the associated Stark quenching of the $2s$ state. For these reasons, we adopted a purely electrostatic confinement scheme which, we later discovered, was first demonstrated in connection with electron space-charge neutralization studies by Kingdon[12] in 1923. Figure 2 shows a cross-sectional view of the apparatus. It is a closed cylinder with a central rod maintained at a negative potential with respect to the grounded cylinder walls. $^3He^+$ ions are created by impact with electrons emitted from a filament located outside the bottom end of the cylinder. The electrons move roughly parallel to the rod at a distance of a few centimeters. The ions which have sufficient angular momentum orbit about the rod in the attractive field and oscillate along its length in the axial well produced by the cylinder ends.

In addition to serving as an ion trap, the rod and cylinder were designed to be a coaxial cavity resonant near $\Delta\nu_2$ with a Q of about 1000. A small coupling loop is inserted partially into one end of the cylinder and excites the TE_{011} mode. This mode has magnetic field components parallel to the rod near the center plane of the cavity which go over to radial components near the ends; there are no azimuthal magnetic field components. The TE_{011} electric field is purely azimuthal. The TM_{111} mode is degenerate with TE_{011}; however, it requires currents across the junctions between the cylinder wall and ends. These are suppressed in our design by a small gap maintained between the end plates and the cylinder. This acts as an im-

pedance which attenuates the TM_{111} currents without materially disturbing the azimuthal TE_{011} currents. The cavity can be tuned slightly by varying the spacing of the end plates on their mounting screws. The ion-trap/cavity dimensions are approximately: length, 34.3 cm; radius, 18.3 cm; and rod diameter, 0.32 cm.

The detectors for the 304-Å photons are 24 stage CuBe venetian-blind-type windowless electron multipliers. Our new results were obtained with these detectors moved about 15 cm closer to the ion trap from their positions shown in our first report.[9] We observed about a factor of 2 increase in the count rate with the new arrangement. The multipliers are shielded by 800-Å-thick aluminum foils which have reasonable transmission for 304-Å photons (about 55%). The foils stop metastable $2\,^1S_0$ and $2\,^3S_1$ He atoms from reaching the multipliers where they would produce a large count rate by surface Auger deexcitation. Auger electrons produced at the foils are stopped by biasing the multipliers so that their first dynode is 150 V negative with respect to the grounded foils.

The state-selection microwave power is generated by a Varian X-12 klystron and broadcast into the ion trap by a horn aimed through a hole in the cylinder wall. This power is on-off modulated by a pin-diode switch under control of the data collection electronics.

The ion trap and multipliers are enclosed in a stainless-steel vacuum chamber whose base pressure is typically about 5.0×10^{-8} Torr. ^{3}He gas is admitted into the chamber from a low-pressure ballast volume through a micrometer-controlled variable leak valve. Normally, we use a pressure of about 3.5×10^{-6} Torr ^{3}He.

The power to excite the hyperfine transition is generated by multiplication and amplification of the output from a Hewlett-Packard 5105A frequency synthesizer. The synthesizer's output frequency at about 270.8 MHz is multiplied by 4 to approach $\Delta\nu_2$. The resulting power is attenuated to an optimum value to excite the transition and is passed into the ion-trap/cavity through an absorptive modulator. The modulator and the synthesizer frequency are automatically controlled by the data collection system. To establish the absolute frequency of the synthesizer, its internal 1.0-MHz crystal oscillator was compared periodically throughout the extent of our measurements to a locally maintained 100-kHz standard which in turn was compared to the 60-kHz broadcasts of WWVB.

A diagram of the data collection scheme and apparatus is shown in Fig. 3. Counts received from the detectors during the B period are stored in 100 channels of a multichannel scalar (MCS). The channel address controls the synthesizer frequency. A typical data cycle consists of a 0.1-msec fill period, during which 200-eV electrons are injected into the trap, followed by A, C, and B periods. The A and B periods are equal and normally set to 50 μsec; the C period, depending on the linewidth desired, has ranged from 0.4 to 1.6 msec. However, our new results were obtained with either $t_C = 0.6$ or 1.2 msec. Following the B period, a 50-μsec dump period occurs during which the rod potential is brought up to ground to allow ions to escape. The sequence is then repeated. Usually the dwell time in a given channel is 1000 data cycles, after which the channel address and synthesizer frequency are incremented. The 100 channels of the MCS are repetitively scanned to accumulate a resonance signal.

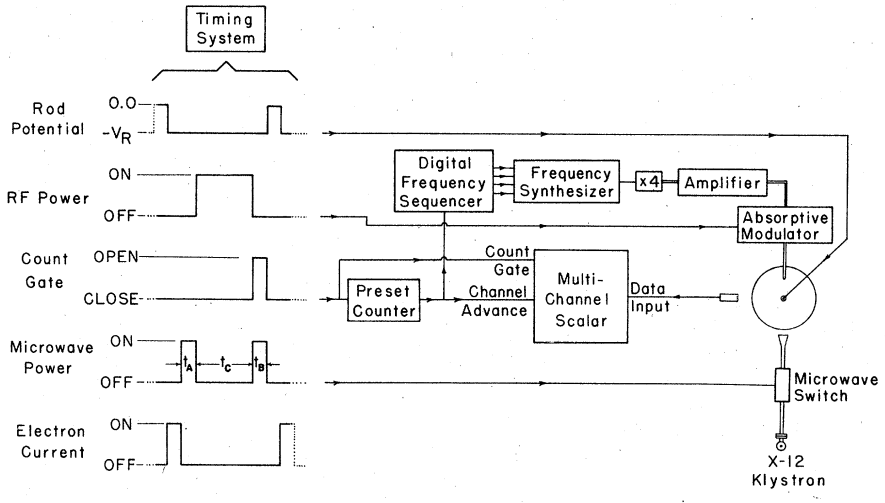

FIG. 3. Data collection and timing scheme.

III. MEASUREMENT PROCEDURE

The ideal of an unperturbed field-free measurement of $\Delta\nu_2$ in $^3He^+$ is only approximated by the device described above. The Earth's magnetic field and the electric field inside the ion trap both cause significant shifts in the resonant frequency. To minimize the effect of magnetic fields we observe the $F=0$ to $F=1$, $m_F=0$ transition, whose field dependence is given by $f(\mathrm{MHz})=\Delta\nu_2+(3.615\times10^{-3})H^2$, where H is in gauss. The Earth's field thus produces about a 1-kHz shift from $\Delta\nu_2$. We use three sets of orthogonal coils to allow arbitrary adjustment of H about $H=0$.

The Stark shift of the $\Delta m_F=0$ resonance is a small but non-negligible effect. It has been calculated by Novick and Commins[8] and we have checked their result. It is due almost entirely to mixing of the $2s$ state with the nearby $2\,^2P_{1/2}$ state. The shift is given by

$$\Delta_E=-(6.6E_{xy}^2+8.8E_z^2), \tag{1}$$

where Δ_E is in Hz and E_{xy} and E_z (the electric fields normal and parallel to the trap axis, respectively) are in V/cm. The ion motion through the trap's nonuniform electric field will result in a shift which is a motional average of the above for any given rod potential. *A priori* calculation of this shift would be difficult due to our ignorance of the details of the ion motion. Our solution has been to make measurements at several rod potentials and to extrapolate the results to zero potential. Thus we have not escaped making an extrapolation; however, as will be seen, the extrapolation is an exceedingly small one.

In terms of the magnet coil currents, I_x, I_y, and I_z, the $\Delta m_F=0$ resonant frequency may be written

$$f=f_0+K_x(I_x-I_x')^2+K_y(I_y-I_y')^2+K_z(I_z-I_z')^2. \tag{2}$$

Our procedure for a given rod potential, is to vary one at a time I_x, I_y, and I_z to determine the constants K_x, K_y, K_z, I_x', I_y', I_z', and f_0. The first three of these are constants for each coil pair, the second three are currents required to cancel the local ambient magnetic field, and f_0 is the zero-magnetic-field resonant frequency uncorrected for the Stark effect, synthesizer offset, and other small systematic effects. These parameters are determined by least-squares fits of the f, I_x (or I_y, or I_z) data to Eq. (8). This field adjustment procedure is done by first setting I_z to produce a field of about 1.0 G and varying I_x and I_y to determine I_x' and I_y'. We then set $I_x=I_x'$, $I_y=I_y'$, and vary I_z to determine f_0.

Line centers are determined by least-squares fits of the resonance signal to the Rabi line shape[13]

$$S(\nu)=AL(\nu)\sin^2[\pi t_c BL(\nu)^{-1/2}]+C, \tag{3}$$

with

$$L(\nu)=B^2/[B^2+(\nu-f)^2]. \tag{4}$$

This yields the parameters A, B, and C, and the line center f. A and C are amplitude and base line parameters; B is the magnetic dipole matrix element in frequency units and is given by

$$B=(\mu_0/2h)(g_J-g_I)H_{\mathrm{rf}}\cos\theta, \tag{5}$$

with θ the angle between the external field and H_{rf} (the oscillating magnetic field of the TE_{011} cavity mode). The minimum H_{rf} required for maximum $S(f)$ occurs for $\theta=0$. Since H_{rf} is predominately parallel to the z axis of the ion-trap/cavity, the resonance signal is optimum for $H_z\gg(H_x^2+H_y^2)^{1/2}$. It is for this reason that we adjust I_x and I_y first.

IV. DATA SUMMARY

During the initial phases of this work, a number of resonance curves were collected under various conditions to establish that the apparatus was per-

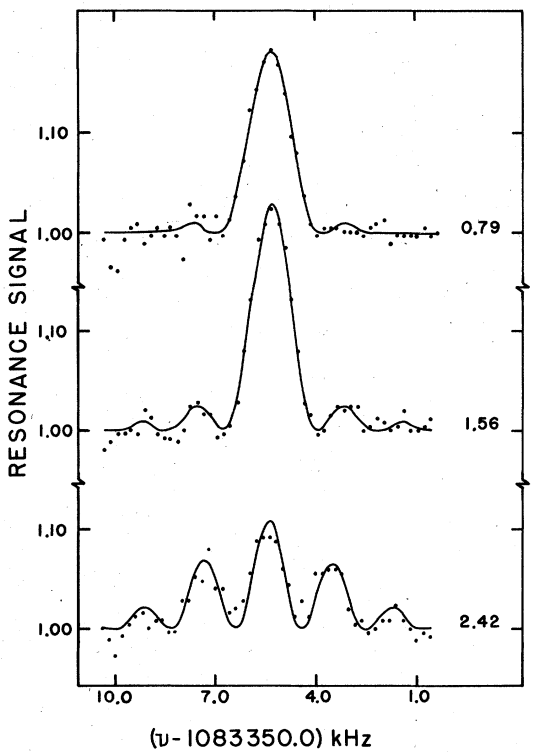

FIG. 4. Resonance curves obtained with differing values of H_{rf}. The curves are least-squares fits of Eq. (3) to the data; the plots are normalized to the fitted baseline. To the right of each curve is the quantity $\pi t_C B$ obtained from the value of B determined by the fit and $t_C=0.6$ msec. The rod potential was $V_R=-4.5$ V and the magnetic field was $H=H_z\simeq0.4$ G.

forming in reasonable conformity to expectations. In particular, data was collected with widely varying values of H_{rf} to check the form for the line shape. Some of these data are shown in Fig. 4. We also collected a series where t_C was varied to display the expected inverse proportionality of the linewidth. These are shown in Fig. 5. Figure 6 shows an example of the measurement sequence used to determine f_0 by variation of I_z. Our final result is derived from a total of 36 such data sets, each of which took about 6 hours of data collection.

The data is summarized in Table I grouped according to the rod potential V_R. Since I_z is measured as a voltage drop across a sense resistor R_z, the field parameters actually determined from f-vs-I_z data are K_z/R_z^2 and $I_z'R_z$, as indicated in Table I. The uncertainties in the f_0 values are those resulting from the counting statistics of the resonance data and were determined by the least-squares line-shape fitting program; they indicate the precision of a single measurement. The quantity Δ_{sw} is the correction to be added to the f_0 values to account for the offset of the frequency-synthesizer internal oscillator with respect to the 60-kHz standard VLF transmission from WWVB; the corrected values are labeled f_0'. We believe

TABLE I. Summary of the data. f_μ is the microwave state-selection frequency. The numbers in the columns labeled f_0 and f_0' are to be added to 1 083 354 000. Hz to obtain f_0 and f_0'.

Data set	V_R (V)	t_C (msec)	f_μ (GHz)	K_z/R_z^2 (Hz/V^2)	$I_z'R_z$ (V)	f_0 (Hz)	Δ_{sw} (Hz)	f_0' (Hz)
61	−4.5	0.6	13.3	249(2)	0.908(15)	938(9)	42	980(9)
62	−4.5	0.6	13.3	249(2)	0.908(16)	945(11)	42	987(11)
63	−4.5	0.6	13.3	248(4)	0.900(25)	930(11)	42	972(11)
64	−4.5	1.2	13.3	247(2)	0.910(14)	945(6)	42	987(6)
72	−4.5	0.6	15.3	242(5)	0.977(36)	948(16)	44	992(16)
73	−4.5	0.6	15.3	250(5)	0.972(34)	933(16)	44	977(16)
74	−4.5	0.6	15.3	246(4)	0.960(27)	938(12)	44	982(12)
75	−4.5	0.6	15.3	250(5)	1.039(30)	946(14)	44	990(14)
76	−4.5	0.6	15.3	252(4)	1.024(28)	935(13)	45	980(13)
77	−4.5	0.6	15.3	249(4)	1.013(28)	932(13)	45	977(13)
93	−4.5	0.6	15.3	250(4)	0.988(24)	931(11)	47	978(11)
94	−4.5	0.6	15.3	240(4)	0.981(25)	945(11)	47	992(11)
95	−4.5	0.6	15.3	245(4)	1.007(26)	935(12)	47	982(12)
96	−4.5	1.2	15.3	245(2)	0.948(17)	937(7)	48	985(7)
							Mean value =	982.9(61)
68	−10.0	1.2	13.3	250(3)	0.976(21)	943(9)	42	985(9)
69	−10.0	1.2	13.3	242(3)	1.005(23)	952(10)	43	995(10)
70	−10.0	1.2	13.3	249(4)	1.007(26)	941(12)	43	984(12)
71	−10.0	1.2	13.3	250(4)	1.025(27)	940(12)	43	983(12)
78	−10.0	0.6	15.3	256(5)	0.998(33)	921(16)	45	966(16)
79	−10.0	0.6	15.3	260(5)	1.040(33)	929(17)	45	974(17)
80	−10.0	0.6	15.3	250(5)	1.003(29)	936(14)	45	981(14)
81	−10.0	0.6	15.3	263(5)	0.985(32)	936(16)	45	981(16)
82	−10.0	0.6	15.3	251(6)	0.950(35)	941(16)	46	987(16)
83	−10.0	0.6	15.3	238(6)	0.952(38)	939(17)	46	985(17)
84	−10.0	0.6	15.3	258(5)	1.007(31)	927(15)	46	973(15)
85	−10.0	0.6	15.3	247(5)	1.005(35)	934(16)	46	980(16)
86	−10.0	0.6	15.3	243(7)	1.038(40)	930(15)	46	976(15)
87	−10.0	0.6	15.3	246(4)	1.008(25)	932(11)	47	979(11)
88	−10.0	0.6	15.3	247(4)	1.015(30)	929(14)	47	976(14)
							Mean value =	980.3(69)
90	−15.0	0.6	15.3	251(5)	1.029(30)	929(14)	47	976(14)
91	−15.0	0.6	15.3	248(5)	1.033(33)	928(16)	47	975(16)
92	−15.0	0.6	15.3	244(5)	1.055(31)	926(14)	47	973(14)
97	−15.0	1.2	15.3	248(3)	0.957(18)	924(8)	48	972(8)
98	−15.0	1.2	15.3	243(3)	0.982(18)	924(8)	48	972(8)
99	−15.0	1.2	15.3	247(2)	0.993(16)	923(7)	48	971(7)
							Mean value =	973.2(19)

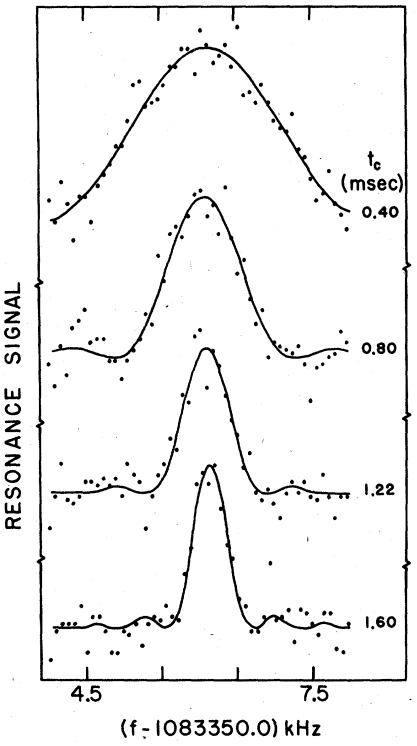

FIG. 5. Resonance curves obtained with differing values of t_C. The rf power was adjusted in each case to hold $t_C B$ approximately constant. The rod potential was $V_R = -4.5$ V and the magnetic field was $H = H_z \simeq 0.6$ G.

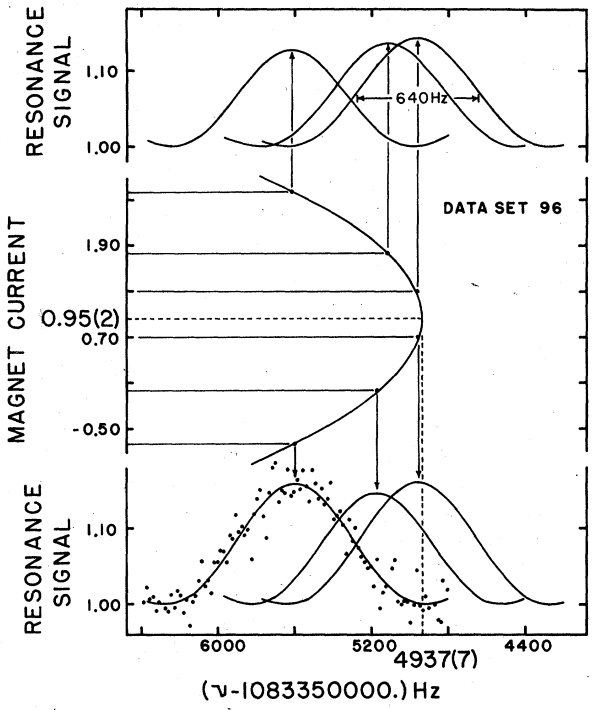

FIG. 6. Variation of resonance line center with current I_z in z axis coil pair. A fit of Eq. (2) to the line center versus magnet current data yields an uncorrected zero-field hfs measurement.

the Δ_{sw} values are accurate to ± 1 Hz. The mean values for the f_0' are unweighted means, and the uncertainty assigned is one standard deviation of a single determination.

V. CORRECTIONS

A. Line-shape asymmetry

We have examined the experimental line shape to determine if any asymmetry exists which might shift the fitted curve, Eq. (3), from the true line center. We believe the true line shape to be symmetric although probably not given precisely by Eq. (3) due to effects such as motional averaging of the rf field amplitude. However, it is possible for asymmetries to be introduced into the data by drifts in one or several of the experimental conditions, or by some unanticipated frequency-dependent effect on the transition rate. To search for such effects in the data, we have combined experimental resonance curves taken under identical conditions in order to gain maximum signal-to-noise ratios for the detection of a possible asymmetry. This procedure is valid since any asymmetry must be consistently present in all similar data in order to produce a net effect on the results. We then fit Eq. (3) to the combined data and examined the residuals, i.e., the difference between the data and the fitted curve. Asymmetry in the data should appear as an asymmetry in a plot of the residuals versus frequency. An example of this procedure is shown in Fig. 7 where six resonances from data sets 72 through 77 have been combined. In all cases studied in this manner, we have detected no asymmetry which would shift the result outside our final error limits.

The $\Delta m_F = \pm 1$ hyperfine transitions might be expected to perturb the line shape, particularly at low magnetic fields. We have detected no evidence of their presence, and this is consistent with the facts that (i) the lowest field at which measurements were made (i.e., data summarized in Table I) was about 70 mG, which would place the $\Delta m_F = \pm 1$ resonances some 50 kHz to either side of the $\Delta m_F = 0$ transition; (ii) the polarization of the rf field was unfavorable to excite $\Delta m_F = \pm 1$ transitions, and (iii) the inhomogeneity of the static field broadened ($\simeq 25$ kHz) and further weakened the $\Delta m_F = \pm 1$ transitions. At most one could expect these resonances to appear as a symmetrically placed, broad, structureless (on the scale of the frequency sweeps) base under the measured line.

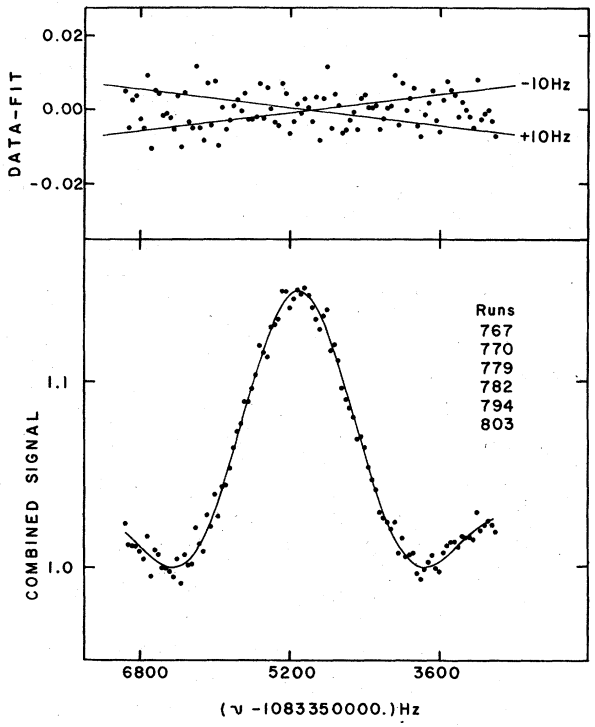

FIG. 7. Plot of combined data and fitted curve, Eq. (3), for six resonances, one each from data sets 72 through 77, taken under identical conditions. The upper plot shows the residuals (data minus fitted curve) versus frequency. The straight lines indicate the slopes required to shift the frequency at which the maximum occurs by ±10 Hz (9 parts per 10^9).

B. Shifts due to magnetic fields

In reality, the line shape, Eq. (3), is modified by the fact that the ions are moving in an inhomogeneous magnetic field, the net effect of the external coils and the Earth's field. If one writes $f = f_0 + kH^2(x, y, z)$ in analogy with Eq. (2), where $H(x, y, z)$ is the magnitude of the net field at position x, y, and z, and further defines $\delta = (\nu - f)/B$, then Eq. (3) becomes

$$S(\delta) = \frac{A}{1+\delta^2} \sin^2[\pi t_c B(1+\delta^2)^{1/2}]. \tag{6}$$

For $t_c B = \frac{1}{2}$ and $\delta \ll 1$ this is well approximated as

$$S(\delta) = A(1-\delta^2). \tag{7}$$

The result of a measurement is an average of S over the ion motion; we denote this as $\langle S\rangle$, and have

$$\langle\delta^2\rangle = (\Delta f^2 - 2k\Delta f\langle H^2\rangle + k^2\langle H^4\rangle)/B^2, \tag{8}$$

where $\Delta f = \nu - f_0$, thus $\langle S\rangle$ is a maximum for $\Delta f = \Delta f_C = k\langle H^2\rangle$ as one might expect. In practice we minimize Δf_C by varying H to produce the minimum $\langle H^2\rangle = \langle H^2\rangle_{\min}$. It is convenient to write $\langle H^2\rangle_{\min} = \langle H_z^2\rangle_{\min} + \langle H_{xy}^2\rangle_{\min}$. We approximate H_z as $H_z = H_z' + H_0(1+az^2)$, where H_z' is the z component of the ambient field in the lab, and the second term approximates the z dependence of the z-axis coil pair with parameters H_0 and a. To lowest order in averages over the ion motion, one has then

$$\langle H_z^2\rangle_{\min} = H_0^2 a^2(\langle z^4\rangle - \langle z^2\rangle^2). \tag{9}$$

For simple harmonic motion of amplitude z_0, one has $\langle z^4\rangle - \langle z^2\rangle^2 = \frac{1}{8} z_0^4$, and as a limiting case for arbitrary motion, $\langle z^4\rangle - \langle z^2\rangle^2 \leq z_0^4$. Thus we expect a shift in the measured hfs due to motional averaging of the z magnetic field of

$$\Delta_z \leq kH_0^2 a^2 z_0^4. \tag{10}$$

We have determined the effect of $\langle H_{xy}^2\rangle_{\min}$ by an experimental technique. At the peak of the resonance curve, Eq. (3) with $\nu = f$, and with the rf field optimized in the sense that $B = \cos\theta/(2t_c)$, the signal S is given by

$$S = A\sin^2(\tfrac{1}{2}\pi\cos\theta) + C. \tag{11}$$

In terms of the magnetic field components, one has

$$\cos\theta = \frac{H_z}{(H_z^2 + H_{xy}^2)^{1/2}}, \tag{12}$$

and one can easily show that Eq. (11) is well approximated by

$$S = A\frac{3H_z^2}{(3H_z^2 + H_{xy}^2)} + C. \tag{13}$$

We further approximate

$$\langle S\rangle = A\frac{3\langle H_z^2\rangle}{(3\langle H_z^2\rangle + \langle H_{xy}^2\rangle)} + C, \tag{14}$$

which may be written in terms of the z-coil current as

$$\langle S\rangle = A\frac{3(I_z - I_z')^2}{3(I_z - I_z')^2 + \Delta I_{xy}^2} + C. \tag{15}$$

This defines the parameter ΔI_{xy} as an effective current which generates H_{xy}.

Thus from a measurement of $\langle S\rangle$ as a function of I_z, one can determine the parameters A, C, and ΔI_{xy}^2. Figure 8 shows some data taken with ν fixed at the resonance peak and I_z varied. This was done for several values of H_{xy}^2 as generated by one of the coil pair currents, I_x. One notes that the half-width of the $\langle S\rangle$-vs-I_z curve has a finite minimum value as I_x is varied; identical behavior occurs for variation of I_y. The minimum half-width $= \Delta I_{\min}$ we take as representing the effect of ion motional averaging of the xy field inhomogeneity. Since $\Delta I_{xy} = 3^{1/2}\Delta I_{\min}$, the resulting shift in the resonance line center is

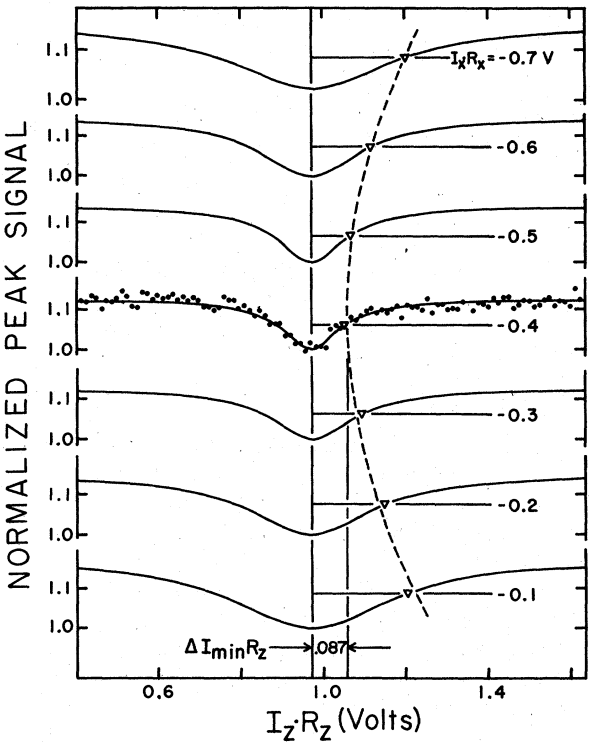

FIG. 8. Variation of resonance peak amplitude with z-axis magnet current for various values of x-axis magnetic field as generated by current I_x. The minimum width of these curves is a measure of the effect of motional averaging of the inhomogeneity in the minimum field normal to the z axis. (see text). For these data, the rod potential was $V_R = -10.0$ V.

$$\Delta_{xy} = 3K_z(\Delta I_{min})^2 . \tag{16}$$

We estimate that for the z-field inhomogeneity contribution, $az_0^2 H_0 < 0.1 H_0$, thus $\Delta_z < 10^{-2} kH_0^2$. However, $kH_0^2 = K_z I_z'^2$; thus,

$$\Delta_z < 10^{-2} K_z I_z'^2 . \tag{17}$$

Typically (see Table I), $K_z/R_z^2 = 250$ Hz/V and $I_z' R_z = 1.00$ V; thus $\Delta_z < 2.5$ Hz; we adopt the value $\Delta_z = 1.3 \pm 1.3$ Hz.

From measurements as shown in Fig. 8, we determined $\Delta_{xy} = 4.5 \pm 2.7$ Hz at $V_R = -4.5$ V and $\Delta_{xy} = 5.7 \pm 3.3$ Hz at $V_R = -10.0$ V; the difference is not significant and we adopt the value $\Delta_{xy} = 5.1 \pm 3.3$ Hz.

The total inhomogeneous field shift, Δ_{IH}, is then $\Delta_{IH} = \Delta_{xy} + \Delta_z$ or $\Delta_{IH} = 6.4 \pm 3.5$ Hz.

A further magnetic shift Δ_H is due simply to our uncertainty in the values I_x' and I_y'. These quantities were measured many times throughout the experiment and their spread of values indicates a positive shift ≤ 1.8 Hz from each. This implies a net shift ≤ 2.5 Hz. We adopt the value $\Delta_H = 1.3 \pm 1.3$ Hz.

The motional magnetic field seen by the confined ions is totally negligible, being $\lesssim 10^{-6}$ G.

C. Shifts due to electric fields

The Stark shift of the hyperfine frequency is given by Eq. (1). This formula is correct only for the case where the magnetic field along the z axis splits the hyperfine Zeeman sublevels by an amount large compared to Δ_E. For the zero magnetic field case the correct expression for Δ_E is the second term in Eq. (1) (since the electric field then determines the z axis). As discussed earlier we do not correct our data with Eq. (1). Rather we plot the mean values of f_0' taken at the three rod potentials $V_R = -4.5$, -10.0, and -15.0 V, vs V_R^2 and extrapolate to $V_R^2 = 0.0$. This is shown in Fig. 9. One sees that the shift with rod potential is of the correct sign and amounts to less than 1.0 Hz at $V_R = -4.5$ V. This is consistent with estimates of the motionally averaged square electric field as well as measurements of the 2s lifetime as a function of rod potential; the shift of this lifetime from its field-free value is sensitive to $\langle E^2 \rangle$. The extrapolated value is $f_0'' = 1083.3549843$ (70) MHz.

The Stark shift due to the cavity electric field can be estimated using Eq. (1) and, in place of E_{xy} or E_z, the averaged cavity field amplitude, E_{rf}. The resonance is optimized for maximum signal amplitude when [see Eqs. (3)–(5)] $H_{rf} t_C g_J \mu_0 / h = 1.0$; for $t_C = 0.6$ msec, and $g_J = 2.0$, one obtains $H_{rf} = E_{rf} = 0.18$ V/cm which implies a shift $\Delta_{EC} = -0.22$ Hz.

D. Pressure shift

Collisions of 2s $^3He^+$ ions with neutral ^3He atoms in the ion trap can cause a shift in the hfs reso-

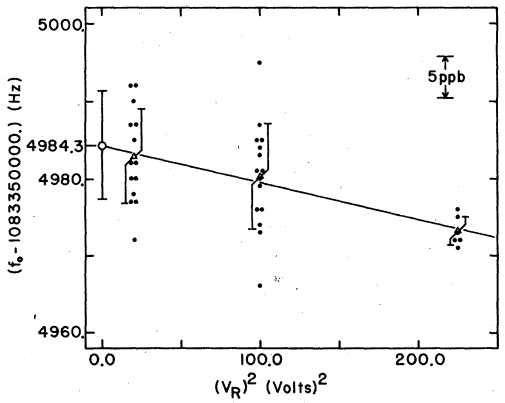

FIG. 9. Extrapolation of line-center measurements to zero rod potential.

nant frequency. A collision can mix into an initially pure $2s$ state some $2p$ amplitude and the differential effect for the two $2s$ hyperfine levels results in a shift in the hfs splitting. The mechanism is the Stark effect in the transient electric field seen by the $2s$ ion during collision. The correction for this effect can be estimated in the following way. The shift caused by collisions with relative velocity v may be expressed as

$$\Delta_{PS} = nv \int_0^\infty P_{2s}(b,v)\beta_{01}(b,v) b\, db\,, \tag{18}$$

where n is the ^{3}He density, $P_{2s}(b,v)$ is the probability of a $2s$ ion surviving a collision, and $\beta_{01}(b,v)$ is the relative phase shift of the hyperfine wave functions produced by a collision with impact parameter b and relative velocity v. A complete treatment would include an average over all relative velocities; however, we estimate the shift using the most probable relative velocity $v = 1.45 \times 10^5$ cm/sec in the zero potential trap. This velocity is a result of the thermal and recoil velocities of the $^3He^+$ ions. $P_{2s}(b,v)$ can be written as

$$P_{2s} = 1 - q(b,v)\,, \tag{19}$$

with $q(b,v)$ the probability of a collision-induced transition to any of the $2p$ levels. This may be estimated with fair precision by the sudden approximation, since the duration of the collision ($b/v \simeq 10^{-12}$ sec) is short compared to the periods ($\simeq 10^{-10}, 10^{-11}$ sec) associated with the $2s$ to $2p$ level splittings. One obtains

$$q(b,v) = \frac{e^2}{\hbar^2} \langle 2p | z_e | 2s \rangle^2 \left[\int_{-\infty}^{\infty} E_z(b,t)\, dt \right]^2, \tag{20}$$

where z_e is the z coordinate of the $^3He^+$ electron, and $E_z(b,t)$ is the z component of the transient electric field seen by the ion during the collision. $E_z(b,t)$ arises, at least at long range, from the ion-atom potential,

$$V(r) = -\eta e/2r^4\,, \tag{21}$$

where η is the polarizability of the atomic partner ($\eta \simeq 0.21 \times 10^{-24}$ cm^3 for He) and r is the ion-atom separation. Choosing the z axis in the plane of the collision and along the line determining b yields,

$$E_z(b,t) = E(b,t)\cos\phi\,, \tag{22}$$

with

$$E(b,t) = 2e\eta/(b^2 + v^2t^2)^{5/2} \tag{23}$$

and

$$\phi = \tan^{-1}(-vt/b)\,, \tag{24}$$

and we have arranged for the collision to occur at $t = 0$.

The result of the integration using a straight-line trajectory and $\langle 2p | z_e | 2s \rangle = 1.5a_0$ yields

$$q(b,v) = (b_c/b)^8\,, \tag{25}$$

for $b > b_c$, and

$$b_c = (4e^2\eta a_0/\hbar v)^{1/4}\,. \tag{26}$$

With our parameters we have $b_c = 5.1$ Å. For $b < b_c$, the true solution for q oscillates between zero and one rapidly as a function of b; furthermore the ion-atom potential has the property that there exists a critical impact parameter b_0, such that for $b < b_0$ the collision partners come together. b_0 is given by

$$b_0 = (4e^2\eta/uv^2)^{1/4}\,, \tag{27}$$

with u the reduced mass of the collision pair. For our case we have $b_0 = 4.4$ Å. It is reasonable, then, that for $b < b_0$ quenching of the $2s$ state is complete and $P_{2s} = 0$ in this region. The ion-atom potential used here of course does not describe the interaction at short range and the partners do not in fact come together; however, since b_0 is considerably larger than the combined radii of the ion and atom in our case, we believe the conclusion that $P_{2s} = 0$ for $b < b_0$ remains valid. In the intermediate region $b_0 < b < b_C$ we set $P_{2s} = \frac{1}{2}$. This procedure yields a quenching cross section of $\sigma_Q = 99.$ Å^2, and a quenching rate, $\sigma_Q nv$, at 3.5×10^{-6} Torr, of 159 sec^{-1} in reasonable agreement with a measured rate of 113 sec^{-1}.

As an estimate of β_{01} we use Eq. (1) for the instantaneous frequency shift in the electric field of the collision, and neglect the small difference between the coefficients of the two field components. Thus,

$$\beta_{01} \simeq 2\pi \int_{-\infty}^{\infty} \Delta_E(b,t)\, dt\,, \tag{28}$$

with $\Delta_E(b,t) \simeq -8E(b,t)^2$, and E in units of V/cm. The result of this calculation, again using a straight-line trajectory, is

$$\beta_{01}(b,v) \simeq -2\pi (b_s/b)^9\,, \tag{29}$$

where

$$b_s^9 = 2.5 \times 10^6\, e^2\eta^2/v\,, \tag{30}$$

and we have $b_s = 3.8$ Å.

Our final result is then

$$\Delta_{PS} = -\tfrac{1}{7}\pi nv b_s^2 [(b_s/b_0)^7 + \tfrac{1}{15}(b_s/b_c)^7]\,. \tag{31}$$

For a ^{3}He pressure of 3.5×10^{-6} Torr, $n = 1.1 \times 10^{11}$ cm^3, and we have as our estimate

$$\Delta_{PS} = -3.8 \pm 3.8 \text{ Hz}\,.$$

We have applied an uncertainty of ± 100% to allow for the high degree of approximation inherent in this calculation.

Since Δ_{PS} is proportional to the product $n\eta^{1/4}$, any reasonable constituent would cause a negligible shift at the 3.0 to 8.0×10^{-8} Torr background pressures present during data collection. In particular, N_2, the principle constituent in our liquid-nitrogen-trapped system, would contribute shifts of $\simeq -0.004$ to $\simeq -0.010$ Hz.

E. Doppler shift

The Doppler effect will manifest itself as sidebands on either side of the resonance signal for ions in periodic motion as discussed by Dicke.[14] In our case, the frequencies of motion are not the same for all ions; they depend on the initial conditions of the ion motion because of the anharmonic potentials and the dependence of the effective radial potential on an ion's orbital angular momentum. The result is a smear of sidebands making up a broad base from which rises a much more intense unbroadened line at the resonance line center. There is the possibility of a shift of the line-center frequency from the rest value, if the ions have a net translational velocity inside the ion trap and if the cavity field contains a running wave component. In our case, this might arise from net radial motion of the initial ion distribution. This can occur through purely elastic ion-ion collisions which change the angular momentum and energy of an ion, thus altering the effective radial potential it sees and changing the equilibrium radius about which it oscillates. Indeed an ion can be lost through such collisions if its angular momentum is reduced to such a small value that it collides with the rod or outer wall of the trap cylinder. If one collision partner is lost, the other remaining confined, a net motion of the charge center can occur. The ion-ion collision time can be estimated from a formula given by Spitzer,[15]

$$\tau_I = 0.78\times10^7 A^{1/2}(kT)^{3/2}Z^{-4}(n_I \ln\Lambda)^{-1}, \qquad (32)$$

where A and Z are the ion mass in atomic units and the charge in units of e, respectively, n_I is the ion density, and kT the effective temperature of the ion plasma in electron volts. Λ is the ratio of the cut-off distance for Coulomb interaction of an ion with its neighbors to the distance of closest approach, $\Lambda \simeq R n_{\max}^{1/3}$ where $n_{\max}$ is the maximum ion density stored, and R is the radius of the trap cylinder (17.8 cm). For our experiment, we estimate $\ln\Lambda \simeq 10.0$, $kT \simeq 1.0$ eV, and $n_I \simeq 10^5$ cm^{-3}. The low value of ion density arises from the fact that the ions spend most of their time near their outer radial turning point. These values yield $\tau_I \simeq 1.3$ sec. An upper limit on the net translation is $\frac{1}{2}R$ so we estimate for the translational velocity $v_d < R/2\tau_I = 7$ cm/sec. An upper limit to the first-order Doppler shift is then $\Delta_{FD} < (v_d/c)\Delta\nu_2 = 0.23$ Hz. Inasmuch as the rf fields in the ion-trap/cavity are nominally standing waves we regard the above estimate as an extreme worst case and do not consider the first-order Doppler shift to be significant in this work.

The second-order Doppler effect will produce a shift $\Delta_{SD} = -(T_I/Mc^2)\Delta\nu_2$ where T_I is the mean ion kinetic energy. T_I will go to a minimum value at $V_R = 0.0$ which corresponds to the mean recoil energy of the 2s $^3He^+$ ions after creation by the electron impact. Thus the extrapolation of the data to $V_R = 0.0$ will remove the contribution due to the trapping field. We estimate at $V_R = -4.5$ V that $T_I = 1.4 \pm 1.0$ eV, which would yield $\Delta_{SD} = -0.5$ Hz; however, at $V_R = 0.0$ we estimate that $T_I \simeq 0.35 \pm 0.20$ eV, which yields $\Delta_{SD} = -0.12 \pm 0.07$ Hz.

VI. RESULTS

In Table II we summarize our results and the corrections discussed above. The final result is

$$\Delta\nu_2 = 1083.354\,980\,7(88)\ \text{MHz}.$$

When taken with the value

$$\Delta\nu_1 = 8665.649\,867(10)\ \text{MHz},$$

from the work of Scheussler *et al.*,[7] one has

$$D_{21}(\text{exp}) = 1.189\,979(71)\ \text{MHz}.$$

The uncertainties in $\Delta\nu_2$ and D_{21} (exp) should be regarded as one-sigma values.

VII. DISCUSSION

The hyperfine structure, $\Delta\nu_n$, in a hydrogenic s state with principle quantum number n, can be

TABLE II. Summary of corrections and results.

Mean values of zero-field line centers	$V_R = -15.0$ V	1083 354 973.2(19) Hz
	$V_R = -10.0$ V	980.3(69)
	$V_R = -4.5$ V	982.9(61)
$V_R^2 = 0$ extrapolated value		$f_0' = 1083\,354\,984.3(70)$
Corrections (to be subtracted from f_0'):		
(a) Motional averaging of inhomogeneous magnetic field		$\Delta_{IH} = 6.4(35)$
(b) Offset of rms-averaged residual field from minimum value		$\Delta_H = 1.3(13)$
(c) rf Stark effect		$\Delta_{EC} = -0.2(1)$
(d) Pressure shift		$\Delta_{PS} = -3.8(38)$
(e) Second-order Doppler shift		$\Delta_{SD} = -0.1(1)$
Net result: $\Delta\nu_2 = 1\,083\,354\,980.7(88)$ Hz		

expressed as[2]

$$\Delta\nu_n = (\Delta\nu_0/n^3)[M/(M+m)]^3(1+b_n+q_n+\delta_n)\,, \quad (33)$$

where M and m are the nuclear and electron masses, respectively, $\Delta\nu_0$ is the nonrelativistic Fermi contact hfs for a point infinite mass nucleus, and b_n, q_n, and δ_n are various correction terms. b_n is the Breit relativistic correction [of order $(Z\alpha)^2$]; q_n stands for the radiative corrections (the largest due to the anomalous electron moment $\simeq \alpha/2\pi$). δ_n represents the effects of nuclear structure and includes various recoil and second-order hfs contributions of order $(Z\alpha)^2$ m/M. $\Delta\nu_0$ is given in frequency units by

$$\Delta\nu_0 = \tfrac{8}{3}\, Z^3\alpha^2 R_\infty c g_I (m/M_p)(I+\tfrac{1}{2})\,, \quad (34)$$

where g_I is the nuclear g factor (in units of μ_{nm}), M_p the proton mass, I the nuclear spin, and R_∞ the Rydberg constant. D_{21} is thus given by

$$D_{21} = \Delta\nu_0\left(\frac{M}{M+m}\right)^3(b_{21}+q_{21}+\delta_{21})\,, \quad (35)$$

where $b_{21} = b_2 - b_1$, etc, and for b_{21}, one has[16]

$$b_{21} = \tfrac{5}{8}(Z\alpha)^2 + \tfrac{179}{128}(Z\alpha)^4 + O(Z\alpha)^6\,. \quad (36)$$

q_{21} is given by[17,18]

$$q_{21} = (\alpha/\pi)(Z\alpha)^2[-3.303\,20\ln(Z\alpha) - 5.5515] + O\alpha(Z\alpha)^3\,. \quad (37)$$

δ_{21} may be partitioned as

$$\delta_{21} = r_{21} + s_{21}\,,$$

where r_{21} contains recoil terms through order $(Z\alpha)^2 m/M$ and effects of the hfs in second order. s_{21} represents everything remaining, principally the uncalculated nuclear size contribution. r_{21} has been calculated by Sternheim[19] who obtained

$$r_{21} = (Z\alpha)^2\,\frac{m}{M}\left[-0.9972\left(1-\frac{ZM_p}{g_I M}\right) - 0.5263\,\frac{g_I}{Z}\right]. \quad (38)$$

The second-order hfs contributions to r_{21} have also been calculated by Schwartz[20] and Douglas.[21]

At the present time, no calculation exists for the remaining term s_{21}; however, estimates of the nuclear size contribution indicate it is of order $(Z\alpha)^2 s_1$ (where s_1 is the nuclear size correction to $\Delta\nu_1$). In hydrogen, s_1 arises from the electromagnetic structure of the proton and is[3] -28.2 ± 2.6 ppm. In $^3He^+$, s_1 is larger and includes terms not present for hydrogen. The most important contribution is the adiabatic correction, i.e., the modification of the electron wave function near the nucleus to account for its adiabatic motion in the force field of the two separated protons. This and several other smaller contributions were calcula-

TABLE III. Summary of theoretical and experimental D_{21} values.

	Fermi hfs $\Delta\nu_0$[Eq. (34)] (MHz)	Reduced mass $[M/(M+m)]^3$	b_{21}(ppm) $5(Z\alpha)^2/8$	$179(Z\alpha)^4/128$	$-1.051\,44\,\alpha(Z\alpha)^2$	q_{21}(ppm) $-1.7671\,\alpha(Z\alpha)^2\ln(Z\alpha)$	r_{21}(ppm) [Eq. (24)]	D_{21}(MHz) Theory	Experiment
H	1421.1579(6)	0.998 367 9	33.282 10	0.003 97	2.010 33	−0.686 68	−0.114 84	0.048 941 32(16)	0.049 13(40) [a]
D	327.234 61(14)	0.999 182 9					−0.028 64	0.011 306 58(4)	0.011 16(16) [b]
$^3He^+$	8661.2475(39)	0.999 454 2	133.128 41	0.063 45	6.908 48	−2.746 74	0.092 02	1.189 801(1)	1.189 979(71) [c]
$^6Li^{++}$	8470.696(42)	0.999 726 3					−0.084 67	2.605 283(13)	
$^7Li^{++}$	29827.13(16)	0.999 765 3	299.538 92	0.321 21	14.053 09	−6.180 16	−0.137 75	9.172 532(50)	

[a] References 1 and 4.
[b] References 5 and 6.
[c] Reference 7 and this work.

ted by Sessler and Foley[22] and are well summarized in the work of Rosner and Pipkin.[23] The net effect is -180 or -143 ppm for the two nuclear wave functions considered and assuming zero contribution from meson currents. Mittleman[24] has argued that nuclear size corrections to the radiative q_{21} terms would be of order $(Z\alpha m/M)^2$.

It is interesting to note that the coefficient of the $(Z\alpha)^2\alpha/\pi$ term in q_{21} has been calculated[17,18] to higher precision than the coefficient of the same term in q_1 (see Ref. 2). The coefficient in q_{21} is $-2.6195-0.9333\pi=-5.5515\pm0.0001$, whereas in q_1 it is 18.36 ± 5.0. Thus the state dependence is better known theoretically than the absolute value.

In Table III we summarize the experimental and theoretical values for D_{21} in H, D, $^3He^+$, and $^{6,7}Li^{++}$; no experimental results are available for the latter. The following values for the required constants were used:

$$c=2.997\,924\,58(12)\times10^{10}\ \text{cm/sec},$$

$$R=1.097\,371\,77(83)\times10^{5}\ \text{cm}^{-1},$$

$$M_p/m=1836.151\,52(70),$$

from the compilation of Cohen and Taylor,[25] and

$$\alpha^{-1}=137.035\,987(29)(0.21\ \text{ppm})$$

from the recent work of Olsen and Williams.[26] For ^3He we used[27]

$$M/m=2.992\,611\,97(30)M_p/m\ (0.01\ \text{ppm}),$$

and

$$g_I=-2.317\,482\,7(5)\times10^{-3}\mu_0\ (0.2\ \text{ppm})$$
$$=-4.255\,249\,3(9)\mu_{nm}.$$

g_I was calculated from measured quantities in the following way:

$$g_I=\frac{g_1'}{g_p''}\,\frac{1+d_{\mathrm{He}}}{1+d_p''}\,(1+d_p')2\,\frac{\mu_p'}{\mu_0}\,, \tag{39}$$

where values used were, for the ratios of the NMR frequencies of ^3He in He to protons in H_2 (Ref. 28):

$$g_I'/g_p''=-0.761\,786\,84\ (0.1\ \text{ppm}),$$

for the proton moment in H_2O in units of the Bohr magneton:[29]

$$\frac{\mu_p'}{\mu_0}=1.520\,992\,983(17)\times10^{-3}\ (11\ \text{parts per}\ 10^9),$$

and for the diamagnetic corrections, ^3He in He (Ref. 28):

$$d_{\mathrm{He}}=59.935\ \text{ppm},$$

protons in H_2 (Ref. 30):

$$d_p''=26.24(18)\ \text{ppm},$$

and protons in H_2O (Ref. 29):

$$d_p'=25.790(14)\ \text{ppm}.$$

The uncertainty in the theoretical values of D_{21} are 0.8 ppm for H, D, and $^3He^+$ from the 0.2-ppm uncertainty in α; for $^{6,7}Li^+$ the uncertainties are $\simeq6$ ppm due to the larger uncertainties in the ^6Li and ^7Li nuclear moments. For $^3He^+$ we have $D_{21}(\text{theory})=1.189\,801(1)$ MHz, and there exists a difference between experiment and theory of $D_{21}(\text{exp})-D_{21}(\text{theory})=178(71)$ Hz. It is anticipated that the next uncalculated term in q_{21} will be of order $\alpha(Z\alpha)^3\Delta\nu_0=197$ Hz which may account for the difference; it may also be attributed, at least in part, to the currently unknown value of s_{21}. Taking $s_1=-162$ ppm (the mean of the two values calculated by Sessler and Foley[22]), then $s_{21}=-1.5\times10^{-4}\,s_1$, would account for the observed difference.

We should like to remark at this point that in the past (e.g., Refs. 4, 6, 17 and 19) when making comparison of hfs values it has been customary to calculate ratios rather than differences, e.g.,

$$R_{21}=8\Delta\nu_2/\Delta\nu_1-1. \tag{40}$$

The advantage of this procedure is that R_{21}(theory) is independent of $\Delta\nu_0$ and the reduced mass factor. The disadvantages are in the increased number of terms in the theoretical expression for R_{21}; these are cross terms between state-independent and -dependent contributions to $\Delta\nu_1$ and $\Delta\nu_2$, many of which are significant at the level of precision attained here. Furthermore, the uncertainty introduced into R_{21} by the uncertainty in state-independent terms can be important at high precisions. For example, in $^3He^+$, the uncertainty in the coefficient (18.5 ± 5.0) of the $(Z\alpha)^2\alpha/\pi$ term in q_1 would cause a 2.5 ppm uncertainty in R_{21} (theory); there is no significant uncertainty in the coefficient of the same term in D_{21}. More significantly the large uncertainty in $s_1(s_1=-162\pm38$ ppm) would introduce a 38 ppm uncertainty in R_{21} (theory). The fractional uncertainty in D_{21}(exp) and R_{21}(exp), as a result of this work, would be the same, 50 ppm, whereas the fractional uncertainty in D_{21}(theory) is 1.0 ppm. It is for these reasons that we prefer to use D_{21} as a vehicle for testing theoretical predictions of $^3He^+$ hfs.

ACKNOWLEDGMENT

Many valuable discussions were held with Dr. Peter J. Mohr on the theoretical aspects of this work; we gratefully acknowledge his assistance.

†Work supported by the U. S. ERDA.

[1]H. Hellwig *et al.*, IEEE Trans. Instrum. Meas. IM-19, 200 (1970).
[2]S. J. Brodsky and G. W. Erickson, Phys. Rev. 148, 26 (1966).
[3]V. W. Hughes, in *AIP Conference Proceedings No.* 26, *High Energy Physics and Nuclear Structure*, edited by D. E. Nagle *et al.* (AIP, New York, 1975), p. 515.
[4]J. W. Heberle, H. A. Reich, and P. Kusch, Phys. Rev. 101, 612 (1956).
[5]S. B. Crampton, *et al.*, Phys. Rev. 141, 55 (1966).
[6]H. A. Reich, J. W. Heberle, and P. Kusch, Phys. Rev. 104, 1585 (1956).
[7]H. A. Schuessler, E. N. Fortson, and H. G. Dehmelt, Phys. Rev. 187, 5 (1969).
[8]R. Novick and E. D. Commins, Phys. Rev. 111, 822 (1958).
[9]M.H. Prior and E. C. Wang, Phys. Rev. Lett. 35, 29 (1975). A less comprehensive report of our subsequent work will appear in *Atomic Physics* 5, *the Proceedings of the Fifth International Conference on Atomic Physics* (Plenum, New York, 1976). The result presented here represents our final analysis of the data and corrections.
[10]M. H. Prior, Phys. Rev. Lett. 29, 611 (1972).
[11]H. Dehmelt, Adv. At. and Mol. Phys. 3, 53 (1967); 5, 109 (1969).
[12]K. H. Kingdon, Phys. Rev. 21, 408 (1923). The possibility of using this type of trap for rf studies of ions was mentioned by H. G Dehmelt, Phys. Rev. 103, 1125 (1956).
[13]N. F. Ramsey, *Molecular Beams* (Clarendon, Oxford, 1956).
[14]R. H. Dicke, Phys. Rev. 89, 472 (1953).
[15]L. Spitzer, Jr., *Physics of Fully Ionized Gases* (Interscience, New York, 1962), p. 133.
[16]We are grateful to Dr. Peter J. Mohr for supplying the $(Z\alpha)^4$ Breit term.
[17]D. E. Zwanziger, Phys. Rev. 121, 1128 (1961).
[18]P. J. Mohr (private communication) has provided an improved value for a numerical integration in Ref. 11.
[19]M. M. Sternheim, Phys. Rev. 130, 211 (1963).
[20]C. Schwartz, Ann. Phys. (N.Y.) 6, 156 (1959).
[21]M. Douglas, Phys. Rev. A 11, 1527 (1975).
[22]A. M. Sessler and H. M. Foley, Phys. Rev. 98, 6 (1955).
[23]S. D. Rosner and F. M. Pipkin, Phys. Rev. A 1, 571 (1970).
[24]M. H. Mittleman, Phys. Rev. 107, 1170 (1957).
[25]E. R. Cohen and B. N. Taylor, J. Phys. Chem. Ref. Data 2, 663 (1973).
[26]P. T. Olsen and E. R. Williams, in *Atomic Masses and Fundamental Constants 5*, edited by J. H. Sanders and A. H. Wapstra (Plenum, New York, 1975).
[27]J. H. E. Mattauch, W. Thiele, and A. H. Wapstra, Nucl. Phys. 67, 1 (1965).
[28]W. L. Williams, V. W. Hughes, Bull. Am. Phys. Soc. 11, 121 (1966).
[29]W. D. Phillips, W. E. Cooke, and D. Kleppner, Phys. Rev. Lett. 35, 1619 (1975).
[30]R. V. Reid, Jr., Phys. Rev. A 11, 403 (1975).